Extensive high-resolution photoassociation spectra and perturbation analysis of the $2(0^-)$ long-range state of ultracold RbCs molecules

Dianqiang Su, Ting Gong, Zhonghua Ji, Yanting Zhao,* Liantuan Xiao, and Suotang Jia
State Key Laboratory of Quantum Optics and Quantum Optics Devices, Institute of Laser Spectroscopy, Shanxi University, Taiyuan 030006, China
and Collaborative Innovation Center of Extreme Optics, Shanxi University, Taiyuan, Shanxi 030006, China

Chuanliang Li†
Department of Physics, School of Applied Science, Taiyuan University of Science and Technology, Taiyuan 030024, China

Jinjun Liu‡
Department of Chemistry and Conn Center for Renewable Energy Research, University of Louisville, Louisville, Kentucky 40292, USA

(Received 17 January 2019; published 22 April 2019)

We report high-resolution photoassociation (PA) spectra of RbCs in the $2(0^-)$ long-range state. Transitions to more than 50 vibrational levels were recorded with the largest binding energy being 507.5 cm^{-1}. By fitting the experimental transition frequencies to the improved LeRoy-Bernstein formula, the C_6 coefficient for the potential energy curve of the $2(0^-)$ state was determined to be -1509 ± 97 a.u.. Perturbation-induced energy level shift and state mixing of the long-range $2(0^-)$ and 3(1) states have been analyzed using an effective Hamiltonian that may be applied to mixing between other excited states of RbCs, as well as other heteronuclear diatomic molecules. Experimentally observed PA transitions to the $v = 190$ vibrational level of the $2(0^-)$ state and a vibrational perturbing level in the 3(1) state have been fit using the effective Hamiltonian, which provides the accurate value of the perturbation coefficient β_0. The experimentally determined rovibronic structure and the deperturbation analysis provide critical information for the search of new schemes for efficient production of ultracold RbCs molecules in the ground state.

DOI: 10.1103/PhysRevA.99.042513

I. INTRODUCTION

In recent years, ultracold molecules have been extensively investigated due to their rich potential applications [1,2]. In particular, ultracold polar molecules have gained increasing attention owing to their long-range, anisotropic, and tunable dipole-dipole interactions. These flexible properties greatly facilitate the applications of ultracold polar molecules in fundamental physics, ultracold chemistry, as well as quantum information and quantum computation [3–5]. Photoassociation (PA) is one of the most-adopted methods for producing ultracold molecules [6]. Ultracold polar molecules, including LiCs, LiRb, NaCs, KRb, RbCs, YbRb, and LiK, have been produced through PA [7–13]. Moreover, for molecules in long-range excited states, PA is an effective technique for investigating the energy level structure near the dissociation limit [5]. Finally, high-resolution PA spectra are also useful for precision measurements [14,15].

Here we report new PA spectra of RbCs in the $2(0^-)$ long-range state (with $\Omega = 0^-$). The RbCs molecule possesses several features that make it a promising candidate for future ultracold physics and chemistry experiments. For example, ground-state RbCs molecules are chemically stable, and the atom exchange reaction that forms homonuclear dimers, $RbCs + RbCs \rightarrow Rb_2 + Cs_2$, is energetically forbidden [16]. The large Franck-Condon factor [17] and electric dipole moment (1.225 D) [18] render quantum computation using trapped RbCs feasible [5]. Production of ground-state RbCs molecules have been realized through magnetoassociation and stimulated Raman adiabatic passage (STIRAP) techniques [18,19]. Dense ensembles of ultracold Rb and Cs could also be used for the investigation of the Bose-Einstein condensation of polar molecules [20,21]. Most recently, a degenerate Fermi gas of polar KRb molecules has been prepared from ultracold atomic gases [22].

Previously, the DeMille Group prepared RbCs molecules in the lowest triplet state, $a^3\Sigma^+$, *via* PA of pairs of colliding Rb and Cs atoms to long-range states just below the $Rb(5S_{1/2}) + Cs(6P_{1/2})$ asymptote, followed by spontaneous emission [23]. The metastable molecules were detected by resonance-enhanced two-photon ionization through the coupled $2^3\Sigma^+$ and $1^1\Pi$ states, which provides details of the vibrational structure of the $a^3\Sigma^+$ state and the intermediate states. In a subsequent work by the same group, RbCs molecules formed in the $a^3\Sigma^+$ state were pumped to a manifold of levels associated with the $c^3\Sigma^+$, $B^1\Pi$, and $b^3\Pi$ states, then dumped to the vibronic ground state, $X^1\Sigma^+(v = 0)$ [11].

*zhaoyt@sxu.edu.cn
†clli@tyust.edu.cn
‡j.liu@louisville.edu

Production of ultracold RbCs molecules in the rovibrational ground state, $X^1\Sigma^+(v=0, J=0)$, was achieved using PA to the $2^3\Pi_0$ state followed by a two-step spontaneous emission progress [24]. Later, high-efficiency production of ultracold RbCs molecules in the rovibronic ground state was achieved *via* PA to a set of three $\Omega = 1$ states followed by spontaneous emission. The maximum production rate was 2×10^3 and 1×10^4 molecules/s when long-range $2^1\Pi_1 - 2^3\Pi_1 - 3^3\Sigma_1^+$ states [25] and short-range $b^3\Pi_1 - c^3\Sigma_1^+ - B^1\Pi_1$ states [26] were chosen to be the intermediate states, respectively. In all cases, mixing between the intermediate states is critical to the efficiency of the population transfer processes. Delocalized character of wave functions of highly excited vibrational levels ensures non-negligible Franck-Condon (FC) factors for spontaneous emission to the vibronic ground level, whereas spin-orbit coupling between the intermediate states enables transitions that circumvent the selection rule due to conservation of the electron spin multiplicity ($\Delta S = 0$). It is therefore desirable to obtain more information of the energy-level structure and mixing mechanism of these intermediate states.

In the present work, we recorded PA transitions to 53 vibrational levels of the $2(0^-)$ state with the largest binding energy being 507.5 cm^{-1}. Many of these transitions are observed for the first time thanks to the improved signal-to-noise ratio of the PA spectra. Rotational constants B_v of accessed vibrational levels were extracted by fitting the recorded transitions. Using the improved LeRoy-Bernstein (LRB) formula [27], we determined the C_6 coefficient for the potential energy curve (PEC) of the $2(0^-)$ state. Spectral analysis reveals that the $v = 190$ vibrational level is perturbed by a vibrational level of the 3(1) state *via* L uncoupling. The degree of wave function mixing between these two states has been determined for each rotational level using experimentally observed transition frequencies.

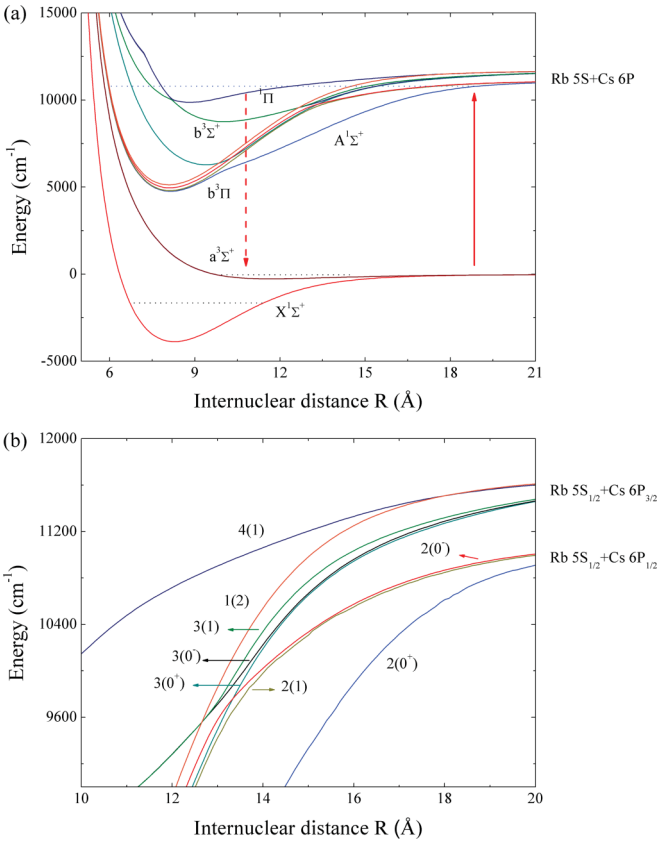

FIG. 1. PA scheme for production of ultracold RbCs molecules. (a) A pair of ^{85}Rb and Cs atoms are excited (red solid arrow) to the $2(0^-)$ state. The formed RbCs molecule then decays spontaneously to its ground state (red dash arrow). (b) Long-range PECs labeled using Hund's case (c) notations. The $2(0^-)$ (red line) and 3(1) (green line) states are mixed with each other.

II. EXPERIMENT

The relevant PECs in the present work are the same as Refs. [28,29] and shown in Fig. 1(a). There the excited states are presented using the Hund's case (a) coupling scheme, corresponding to the case of short-range interaction. Figure 1(b) illustrates details of the long-range PECs labeled using Hund's case (c) notations.

The present experiment used a dual-species dark magneto-optical trap (MOT) that simultaneously decreased the collision rate and increased the density of trapped atoms [30–32]. The final atomic temperature was about 46 μK and the background pressure was 5×10^{-7} Pa. Colliding ^{85}Rb and Cs atomic pairs were resonantly excited by PA to the long-range $2(0^-)$ state below the $^{85}\mathrm{Rb}(5S_{1/2}) + \mathrm{Cs}(6P_{1/2})$ asymptote. Following PA, a fraction of the excited molecules decayed to the ground triplet states $a^3\Sigma^+$ through spontaneous emission and the rest dissociated to free ^{85}Rb and Cs atoms with high kinetic energy.

A continuous-wave tunable Ti:sapphire laser (SolsTiS, M Squared) with a typical linewidth of 100 kHz and intensity of $\sim$194 W/cm^2 was used as the PA laser. Its scan rate was set as 30 MHz/s. The laser frequency was measured with an absolute (relative) accuracy of 60 MHz (2 MHz) using a wavelength meter (WS7-60, HighFinesse).

Two cameras (FL3-GE-03S1M-C, Point Grey) mounted with color filters were placed to separately detect the trap-loss fluorescence of ^{85}Rb and Cs, which represents the formation of ultracold RbCs molecules. The cameras were also used to monitor spatial overlap of the two dark MOTs. Several measures have been taken to improve the signal-to-noise ratio. The long exposure time (60 ms) of both cameras effectively eliminates high-frequency noise in fluorescence detection. The application used to subtract background noise in the image processing suppresses the scattering light from trapping atoms. Using a glass cell to trap the ultracold atoms makes a more stable magnetic field and provides a higher collecting efficiency of atomic fluorescence than using metal chambers. Ultimately, the fluorescence signals from both cameras have fluctuation less than half a percent. The low noise level of the fluorescence signal contributes to the relatively high signal-to-noise ratios of the PA spectra in the present work.

III. RESULTS

A typical PA spectrum with the vibrational quantum number $v = 156$ in the $2(0^-)$ state is shown in Fig. 2, in which

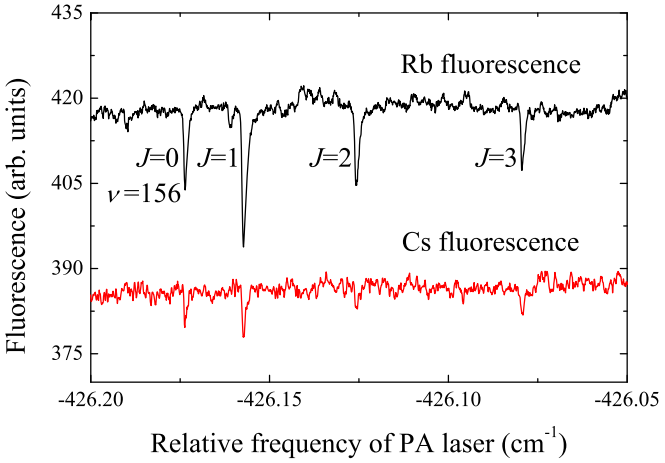

FIG. 2. A typical PA spectrum with $v = 156$ in the $2(0^-)$ state. The x axis indicates the excitation frequency relative to the $^{85}\mathrm{Rb}(5S_{1/2}) + \mathrm{Cs}(6P_{1/2})$ asymptote at 11178.4172 cm^{-1}, i.e., the binding energy of excited RbCs molecules. Dips in the fluorescence spectra of Rb and Cs atoms are due to formation of RbCs molecules by PA.

the rotational quantum number J is labeled for each observed transition. Maximum J value for most observed vibronic transitions is limited to 3 owing to the low temperature. In the present paper, transition frequencies are presented as relative to the $\mathrm{Rb}(5S_{1/2}) + \mathrm{Cs}(6P_{1/2})$ asymptote at 11178.4172 cm^{-1}, i.e., equal to the binding energies of excited RbCs molecules.

A. Rotational structure and rotational constants

For a nonrigid diatomic molecule, relative energies of rotational levels in a vibrational or vibronic state are [33]

$$E_{vJ}/hc = B_v J(J+1) - D_v J^2(J+1)^2 (J \geqslant 0), \qquad (1)$$

where B_v and D_v are the rotational constant and the centrifugal distortion constant of the vibrational level, respectively. To get high-resolution rovibrational energy levels, much more complicated vibrational Hamiltonian analysis is needed [34,35].

In the present work, centrifugal distortion is neglected due to low J values for the observed transitions. Rotational constants B_v of the accessed vibronic states were obtained by fitting the experimentally determined PA transition frequencies to Eq. (1), and are listed in Table I. Uncertainties of B_v's are on the order of 10^{-5} cm^{-1}. Previous experimental [36] and theoretical [37] values are also listed for comparison. In this work, in total 53 vibrational levels of the $2(0^-)$ state are assigned with $v = 151 - 208$ based on previous calculations [37], although transitions to several vibrational levels within this range were not observed due to small FC factors or mixing with hyperfine-rotational substructure of $\Omega \neq 0$ states [36]. The observed transition frequencies and fit rotational constants agree well with theoretical calculations.

B. Potential energy curve

Binding energies of vibrational levels can be described by the improved LeRoy-Bernstein (LRB) formula [27]:

$$D - E_v \approx \left(\frac{v_D - v}{H_n^{-1}}\right)^{2n/(n-2)} \times \left[1 - \frac{2n}{n-2}\gamma\left(\frac{v_D - v}{H_n^{-1}}\right)^{2n/(n-2)-1}\right], \qquad (2)$$

where

$$H_n^{-1} = \sqrt{\frac{2\mu}{\pi}}\frac{(-C_n)^{1/n}}{\hbar(n-2)}\frac{\Gamma\left(\frac{n+2}{2n}\right)}{\Gamma\left(\frac{n+1}{n}\right)}. \qquad (3)$$

In Eq. (2), $D - E_v$ is the binding energy for a vibrational level with vibrational quantum number v, v_D is the extrapolated noninteger value of v at the dissociation limit, H_n^{-1} is a parameter related to the C_n coefficient, γ is an extra parameter in the correction term appended to the conventional LRB formula [38], and μ is the reduced mass of the molecule.

Near the dissociation limit, the internuclear interaction can be expressed as $V(R) \approx D + \sum_n \frac{C_n}{R^n}$ [27], where R is the internuclear distance, and n's are integers. For heteronuclear molecules, the internuclear interactions are dominated by the van der Waals potential that is inversely proportional to the sixth power of R. Therefore, only the $n = 6$ term is chosen in the present work.

Experimentally determined binding energies of all accessed vibrational levels are fit to LRB [38] and improved LRB [27] relations. The results are shown in Fig. 3(a), in which the insert indicates the residuals of the two fits. Using the conventional LRB formula, the C_6 coefficient is deduced to be -7500 ± 500 a.u.. Using the improved LRB formula [Eq. (2)], the C_6 coefficient is determined to be -1509 ± 97 a.u. with $\gamma = 0.0140 \pm 0.0002$. In addition, using the same formula, v_D is determined to be 221.7 ± 0.2, which agrees with the theoretically calculated vibrational level $v = 221$, which has a binding energy of $D - E_v = 0.0137$ cm^{-1} (not shown in Table I) [37].

C. Irregularity in rotational constants and perturbation analysis

Rotational constants B_v for all accessed vibrational levels are plotted in Fig. 3(b). Comparing with the previous work at Yale [23], the discrepancies are small (<0.00034 cm^{-1}) and can be attributed to the limited precision of the wavelength meter. Notably, experimentally determined B_v values are significantly irregular than the calculated ones. This is attributed to perturbation by neighboring electronic states *via* L uncoupling [39].

In the Hund's case (c) coupling scheme, there are three electronic states that converge to the $\mathrm{Rb}(5S_{1/2}) + \mathrm{Cs}(6P_{1/2})$ asymptote: $2(0^+)$, $2(1)$, $2(0^-)$ (see Fig. 1(b)), and five to the $\mathrm{Rb}(5S_{1/2}) + \mathrm{Cs}(6P_{3/2})$ asymptote: $3(0^-)$, $3(1)$, $3(0^+)$, $4(1)$, $1(2)$. In order to identify possible perturbers, it is worth noting that all excited states in the Hund's case (c) representation can be expanded using eigenfunctions in the Hund's case (a) or (b) representations [40,41]. Possible Λ "parent states" for the aforementioned Hund's case (c) states are listed as

TABLE I. Observed rovibrational transition frequencies and fit rotational constants of the $2(0^-)$ state of ^{85}RbCs.

	This work					Ref. [36]		Ref. [37]	
v	J=0 (cm^{-1})	J=1 (cm^{-1})	J=2 (cm^{-1})	J=3 (cm^{-1})	B_v (exp) (cm^{-1})	J=0 (cm^{-1})	B_v (exp) (cm^{-1})	J=0 (cm^{-1})	B_v (theory) (cm^{-1})
208	−6.0901	−6.0857	−6.0798	−6.0679	0.00182	...	...	−5.9932	0.00182
207	−7.3555	−7.3516	−7.3438	−7.331	0.00204	...	...	−7.2613	0.00195
206	−8.7787	−8.7746	−8.7661	−8.7515	0.00227	...	...	−8.6995	0.00208
205	−10.3235	−10.3182	−10.3074	...	0.00269	...	...	...	0.00241
204	−12.3323	−12.3266	−12.3158	−12.2979	0.00286	−12.331	0.0027	−12.1296	0.00235
203	−14.2501	−14.2445	−14.2336	−14.2176	0.0027	...	...	...	0.00247
202	...	...	...	...	...	...	...	−16.3515	0.00261
201	−18.7995	−18.7941	−18.7833	−18.7676	0.00266	−18.794	0.0027	−18.7824	0.00274
200	−21.3992	−21.3928	−21.3807	−21.3637	0.00295	−21.408	0.0028	−21.436	0.00287
199	−24.2112	−24.2408	−24.1926	−24.1733	0.00315	−24.212	0.003	−24.32	0.00301
198	−27.1408	−27.1327	−27.1167	−27.0941	0.00389	−27.144	0.004	−27.4057	0.00406
197	−30.6885	−30.6818	−30.6681	...	0.0034	−30.698	0.0035	−30.8105	0.00327
196	−34.2078	−34.2009	−34.0187	−34.1664	0.00345	−34.216	0.0034	−34.4225	0.0034
195	−38.0083	−38.001	−37.9871	−37.9644	0.00364	−38.026	0.0036	−38.2917	0.00353
194	−42.0481	−42.0406	−42.0249	−42.002	0.00385	...	...	−42.4135	0.00366
193	−46.5628	−46.5549	−46.5386	−46.5149	0.00395	−46.574	0.0039	−46.8063	0.0038
192	−51.0905	−51.0820	−51.0673	−51.0434	0.00393	−51.099	0.004	−51.4539	0.00391
191	−55.9743	−55.966	−55.9496	−55.9253	0.00408	−55.98	0.0041	−56.346	0.00404
190	−61.0714	−61.0722	−61.0444	−61.0178	0.00482	−61.074	0.0046	−61.5179	0.00421
189	−66.7142	−66.7057	−66.6884	−66.6624	0.00432	...	...	−66.9616	0.00426
188	−72.4707	−72.4616	−72.4434	−72.4164	0.0045	...	...	−72.5737	0.00436
187	−77.9542	−77.9483	−77.9248	...	0.00504	−78.485	0.0047	−78.4133	0.00448
186	−84.984	−84.9757	−84.9569	−84.9294	0.0046	−84.8924	...	−84.5485	0.0046
185	−91.6711	−91.6614	−91.6426	−91.6121	0.00491	...	...	−90.9488	0.00472
184	−98.0251	−98.0107	−97.9818	−97.9386	0.00529	...	...	−97.624	0.00491
183	−106.044	−106.032	−106.015	−105.979	0.00533	...	...	−104.644	0.00497
182	−113.667	−113.658	−113.635	−113.603	0.00533	−113.561	...	−111.933	0.00509
181	−121.708	−121.697	−121.676	−121.644	0.00526	−121.603	...	−119.55	0.00523
180	−130.002	−129.991	−129.97	...	0.00535	...	...	−127.45	0.00534
179	−138.645	−138.634	−138.612	−138.578	0.00558	...	...	−135.579	0.00578
178	−147.602	−147.592	−147.569	−147.534	0.00567	...	...	−144.155	0.00557
177	−156.896	−156.881	−156.859	...	0.00613	...	...	−152.948	0.00571
176	−167.57	−167.558	−167.53	−167.49	0.00665	...	...	−162.101	0.00581
175	−176.454	−176.443	−176.421	−176.382	0.00611	−176.333	...	−171.522	0.00593
174	−186.736	−186.72	−186.696	−186.658	0.00622	−186.611	...	−181.273	0.00604
173	−196.899	−196.888	−196.859	...	0.00677	...	...	−191.308	0.00616
172	−208.257	−208.243	−208.217	−208.179	0.00643	...	...	−201.676	0.00626
171	−219.534	−219.521	−219.495	−219.456	0.0065	...	...	−212.326	0.00639
170	−231.044	−231.03	−231.003	−230.963	0.00671	...	...	−223.312	0.00648
169	−243.014	−243	−242.974	...	0.00675	...	...	−246.153	0.0067
168	−255.501	−255.485	−255.458	−255.412	0.00736	...	...	−258.042	0.00681
167	−267.757	−267.742	−267.714	−267.672	0.00702	...	...	−270.23	0.00691
166	...	...	...	...	...	...	...	−282.724	0.00702
165	−293.52	−293.603	−293.575	−293.535	0.00705	...	...	−295.518	0.00712
164	−307.345	−307.33	−307.301	−307.256	0.00742	...	...	−308.619	0.00722
163	−321.408	−321.392	−321.361	−321.316	0.00761	...	...	−322.017	0.00733
162	...	...	...	...	...	...	...	−335.704	0.00743
161	−349.777	−349.753	−349.723	−349.677	0.00818	...	...	−349.703	0.00753
160	−364.889	−364.873	−364.84	−364.793	0.00799	...	...	−364.034	0.00766
159	−379.338	−379.322	−379.291	−379.243	0.00786	...	...	−378.602	0.00773
158	...	...	...	...	...	...	...	−393.496	0.00783
157	−410.9	−410.888	−410.857	−410.807	0.00788	...	...	−408.756	0.00799
156	−426.203	−426.186	−426.153	−462.104	0.00824	...	...	−424.175	0.00803
155	−442.754	−442.734	−442.704	−442.655	0.0082	...	...	−439.97	0.00812
154	...	...	...	...	...	...	...	−456.093	0.00823
153	−475.387	−475.37	−475.334	−475.282	0.00875	...	...	−472.434	0.00832
152	−493.183	−493.167	−493.132	−493.0814	0.00855	...	...	−489.121	0.0084
151	−507.554	−507.537	−507.502	...	0.00866	...	...	−506.108	0.0085

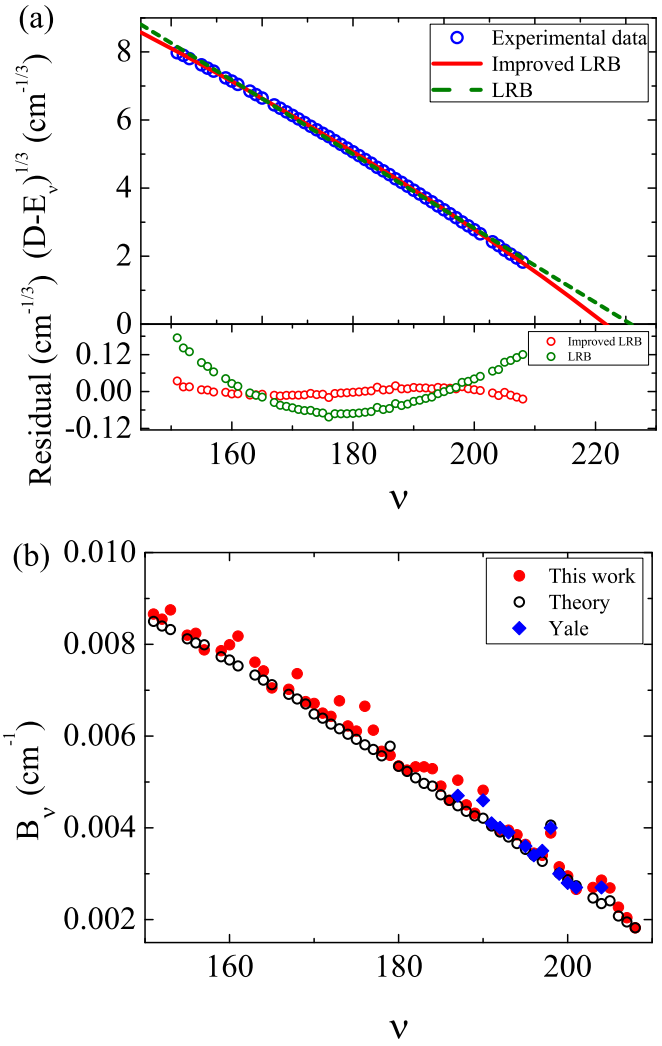

FIG. 3. (a) Binding energy $(D - E_v)^{1/3}$ as a function of the vibrational quantum number v in the long-range $2(0^-)$ state. Experimentally determined values (blue circles) are compared with fits using the LRB (green dashed line) and improved LRB (red solid line) models. X axis intercepts of the fit lines are fit values for v_D. Inset shows residuals of the fits. (b) Rotational constant B_v as a function of the vibrational quantum number v.

follows [29]:

$\Omega = 0^+$: $^1\Sigma^+$, $^3\Pi$;
$\Omega = 0^-$: $^3\Sigma^+$, $^3\Pi$;
$\Omega = 1$: $^3\Sigma^+$, $^1\Pi$, $^3\Pi$;
$\Omega = 2$: $^3\Pi$.

The $2(0^-)$ state is dominated by the $1^3\Pi_{0^-}$ component. Angular momentum selection rules for rotational perturbation introduced by the L uncoupling have been outlined in previous works [40]. Note that $\Omega = 0^+$ and $\Omega = 0^-$ states do not mix for symmetry reasons [42]. Following these selection rules the only Hund's case (a) states that may perturb the $^3\Pi_{0^-}$ state are $^3\Sigma^+_{0^-}$ and $^3\Sigma^+_1$. Among the states converging to $\mathrm{Rb}(5S_{1/2}) + \mathrm{Cs}(6P_{1/2,3/2})$ limits, the $^3\Sigma^+_{0^-}$ and $^3\Sigma^+_1$ states mainly contribute to the $3(0^-)$ and $3(1)$ states in the Hund's case (c) representation, respectively. Perturbation between the $^3\Pi_{0^-}$ and $^3\Sigma^+_{0^-}$ (with $\Delta\Omega = 0$) shifts all rotational energy levels by the same magnitude and is absorbed in the vibronic term value. Perturbation between the $^3\Pi_{0^-}$ and $^3\Sigma^+_1$ states is J dependent and hence alters the rotational structure. Therefore, in the present work, we consider only perturbation between the $2(0^-)$ and $3(1)$ states, dominated by the $^3\Pi_{0^-}$ and $^3\Sigma^+_1$ components, respectively. The off-diagonal matrix elements of the effective Hamiltonian due to this perturbation is [40,41,43]

$$\langle J, v, ^3\Pi_{0^-}|H|J', v', ^3\Sigma^+_1\rangle = \mp\beta_0[J(J+1)]^{1/2}\delta_{JJ'} \qquad (4)$$

where

$$\beta_0 = \langle v, ^3\Pi_{0^-}|\mathbf{B}L_+|v', ^3\Sigma^+_1\rangle = \langle v|\mathbf{B}|v'\rangle\langle ^3\Pi_{0^-}|L_+|^3\Sigma^+_1\rangle. \qquad (5)$$

In Eq. (4), $\mp$ is for the positive and negative parity combination of the rotational energy levels [40]. In Eq. (5), $\mathbf{B}$ is the rotational constant operator. $L_\pm$ are the raising and lowering operators for the electron orbital wave function. The second equality in Eq. (5) assumes that the electronic factor is independent of the vibrational quantum numbers.

An effective Hamiltonian matrix has been constructed and used for fitting and deperturbing the observed PA spectra. Its diagonal elements consist of the rotational Hamiltonian for a rigid rotor, while its off-diagonal elements describe perturbation between the $2(0^-)$ and $3(1)$ states [Eq. (4)].

As indicated by the irregularity in the experimentally determined rotational constants [Fig. 3(b)], many accessed vibrational levels of the $2(0^-)$ state are perturbed. A precise deperturbation analysis requires experimental observation of transitions to both electronic states that are involved. Unfortunately, only one vibrational level of the $3(1)$ state was accessed in our experiment by PA due to the weak signal. It is in the proximity of the $v = 190$ level of the $2(0^-)$ state, separated by ~ 1 cm^{-1}. No definitive vibrational assignment can be made to this solely accessed vibrational level of the $3(1)$ state. Fitting rotational structure in PA transitions to the $2(0^-)$ ($v = 190$) and the perturbing vibrational level of the $3(1)$ state simultaneously allows quantitative analysis of mixing between these two electronic states. It is assumed that these two levels are free from other rotational perturbations.

In Fig. 4, spectra of PA transitions to both vibronic levels are shown. All pairs of transitions with $J = 0, 1, 2, 3$ are fit simultaneously. β_0 is determined to be 0.0142 ± 0.0026 cm^{-1} and the rotational constant of the perturbing vibrational level in the $3(1)$ state is $B_v = 0.0044 \pm 0.0001$ cm^{-1}. Calculated transition frequencies with and without perturbation are marked with red solid and blue dashed lines, respectively. They are also listed in Table II in Appendix A.

Mixing ratios of the $2(0^-)$ and $3(1)$ states for all J values can be derived from the eigenvectors of the effective Hamiltonian and are plotted in Fig. 5. In Fig. 5, $C[^3\Pi_{0^-}]$ and $C[^3\Sigma^+_1]$ are coefficients for the $^3\Pi_{0^-}$ and $^3\Sigma^+_1$ basis states, respectively, in the eigenvectors of the effective Hamiltonian. Because rotational constants of these two levels are close, the unperturbed energy separation between rotational levels with the same J value does not change significantly. The mixing ratio is therefore mainly determined by the coupling strength, i.e., the off-diagonal matrix element in the effective Hamiltonian [Eq. (4)], which is strongly J dependent.

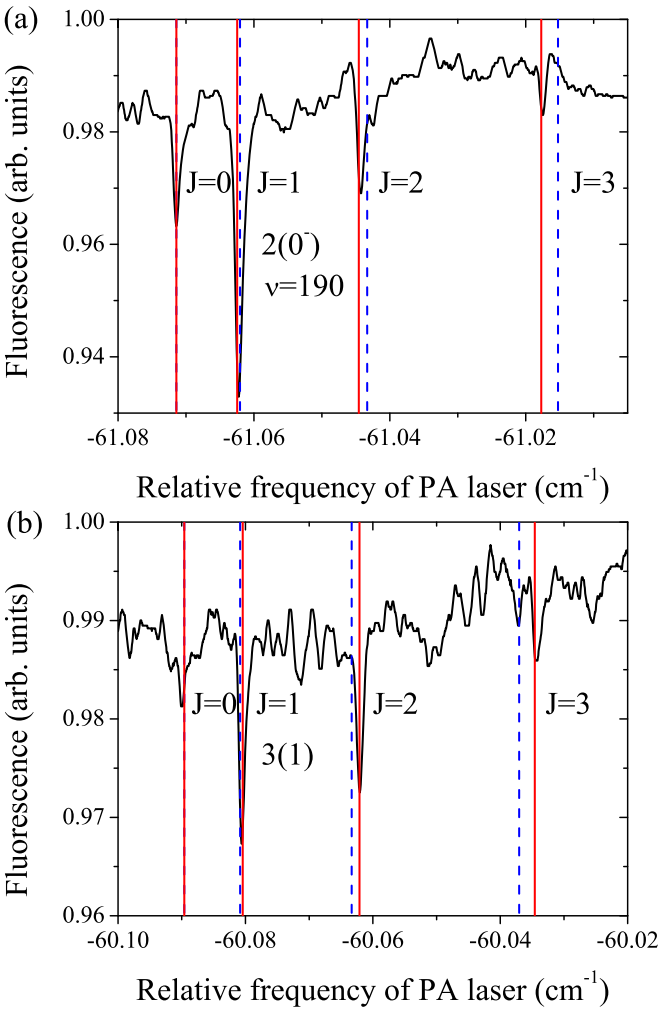

FIG. 4. (a) Trap loss signal of the $2(0^-)$ state. The calculated energy eigenvalues with and without perturbation are denoted by red solid and blue dashed lines, respectively. (b) Trap loss signal of the 3(1) state. Only Rb trap loss signals are shown for clarity. PA transitions of Cs have identical transition frequencies and similar intensities as Rb.

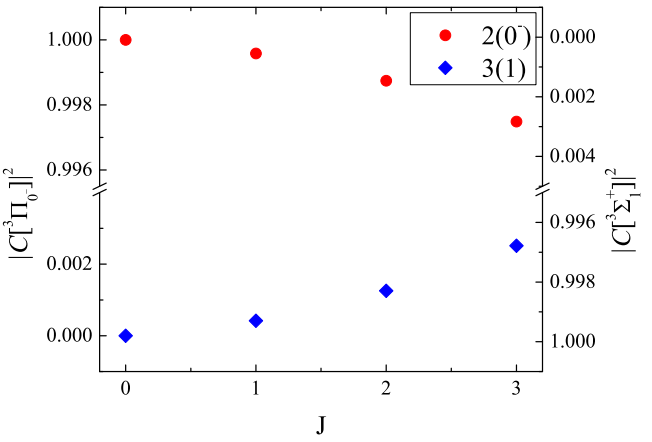

FIG. 5. Mixing of the $2(0^-)$ and 3(1) states for rotational quantum numbers $J = 0, 1, 2, 3$.

IV. DISCUSSION AND CONCLUSIONS

In conclusion, we have obtained high-resolution PA spectra of RbCs in the $2(0^-)$ long-range state, in which transitions to many vibrational levels were observed for the first time. By fitting the rotational energy level structure to the improved LRB formula [27], the C_6 coefficient for the PEC of the $2(0^-)$ state was determined to be -1509 ± 97 a.u., with the correction parameter γ being 0.0140 ± 0.0002. Irregularity in the rotational constants B_ν for different vibrational levels of the $2(0^-)$ state is attributed to perturbation by and mixing with the 3(1) state *via* L uncoupling. Quantitative deperturbation analysis has been done by fitting the observed rovibronic transitions to an effective Hamiltonian. The shift of energy levels and mixing ratios of wave functions of the long-range $2(0^-)$ and 3(1) states have been determined in the deperturbation process. The present work provides the detailed rovibronic structure of RbCs in the $2(0^-)$ long-range state and quantitative information of the mixing between the $2(0^-)$ and 3(1) states, both of which are critical to increasing the PA rate and efficiency of population transfer. Therefore, results from the present work are of great significance to the search of new schemes for production of ultracold RbCs molecules in the ground state. The effective Hamiltonian used in the present work can be used for deperturbation analysis of mixing between other states of RbCs as well as other heteronuclear diatoms.

In the present work, only one vibrational level of the 3(1) state has been accessed. Deperturbation analysis is therefore limited to mixing between this vibrational level and its neighboring $2(0^-)$ ($\nu = 190$) level. Experimental PA or other types of spectra of transitions to more vibrational levels of the 3(1) state are strongly desired so that more comprehensive analysis of mixing between these two electronic states can be achieved.

TABLE II. Experimental frequencies of PA transitions to the $2(0^-)$ (ν=190) level and the perturbing 3(1) vibrational level in comparison with those calculated with and without perturbation [Eq. (4)]. The transition frequencies are relative to the $Rb(5S_{1/2}) + Cs(6P_{1/2})$ asymptote at 11178.4172 cm^{-1}.

	$2(0^-)$			3(1)		
J	Experiment (cm^{-1})	Fit without perturbation (cm^{-1})	Fit with perturbation (cm^{-1})	Experiment (cm^{-1})	Fit without perturbation (cm^{-1})	Fit with perturbation (cm^{-1})
0	−61.07144	−61.07141	−61.07141	−60.09005	−60.08960	−60.08960
1	−61.06223	−61.06205	−61.06246	−60.08055	−60.08084	−60.08043
2	−61.04421	−61.04333	−61.04456	−60.06204	−60.06332	−60.06209
3	−61.01745	−61.01525	−61.01771	−60.03443	−60.03704	−60.03459

Previously, ground electronic state ($X^1\Sigma^+$) RbCs molecules were formed *via* spontaneous emission following PA, dominantly to the excited vibrational levels due to favorable FC constants [36]. In Ref. [36], it is estimated that the majority of the ground electronic state RbCs molecules were formed on vibrational levels with v around 62 at a rate of $\sim 5\times 10^5$ molecules/s. In the present work, PA transitions to higher vibrational levels were utilized to form cold RbCs. The rate of forming ground electronic state molecules is expected to be close to but larger than that reported in Ref. [36] due to stronger coupling between different electronic states at higher vibrational levels.

In a separate experiment in our lab, formation of ground vibronic state ($X^1\Sigma^+$, $v = 0$) RbCs molecules was detected directly using $1 + 1$ resonance-enhanced-multiphoton ionization (REMPI) spectroscopy. RbCs molecules on the lowest rotational levels of the ($X^1\Sigma^+$, $v = 0$) were excited to the $v = 12$ level of the $2^1\Pi$ state using a Nd:YAG (532 nm) pumped pulsed dye laser at 651.8 nm, and ionized using the second photon (651.8 nm) of the dye laser. REMPI spectra with the PA transition to the $v = 190$ level of the $2(0^-)$ state and the unassigned perturbing vibrational level of the 3(1) state are given in Appendix B. The REMPI ion signal provides a direct measure of formation of the ground vibronic state RbCs molecules. Using the method outlined in Refs. [44,45], we estimate that formation of ground vibronic state RbCs molecules *via* spontaneous emission following PA in the present experiment has a rate on the order of 10^3 molecules/s.

ACKNOWLEDGMENTS

We acknowledge Professor R. W. Field (MIT) for helpful discussions and T. Bergeman for the theoretical data. This work was supported by National Key R&D Program of China (Grant No. 2017YFA0304203), Natural Science Foundation of China (Grants No. 61675120, No. 11434007, No. 61875110, and No. U1810129), NSFC Project for Excellent Research Team (Grant No. 61121064), '1331 KSC', PCSIRT (Grant No. IRT 17R70), and 111 project (Grant No. D18001). J.L. acknowledges financial support from the NSF under Grant No. CHE-1454825.

APPENDIX A: FREQUENCIES OF PA TRANSITIONS

PA transitions to the $2(0^-)$ and 3(1) states are calculated with and without perturbation, which are list in Table II. The experimental data are also attached for comparison.

APPENDIX B: REMPI SPECTRA

RbCs molecules ($X^1\Sigma^+$, $v = 0$) were excited to the $v = 12$ level of the $2^1\Pi$ state using a Nd:YAG (532 nm) pumped pulsed dye laser at 651.8 nm, and ionized using a second photon (651.8 nm) of the dye laser. The ions formed in this process were accelerated by a pulsed electric field. Then, the ions were detected by a pair of microchannel plates (MCPs). The ion signal was detected, amplified, then monitored on a digital oscilloscope and simultaneously recorded by an NI PCI-1714 card following a boxcar (Boxcar, SRS-250) with 10 averages.

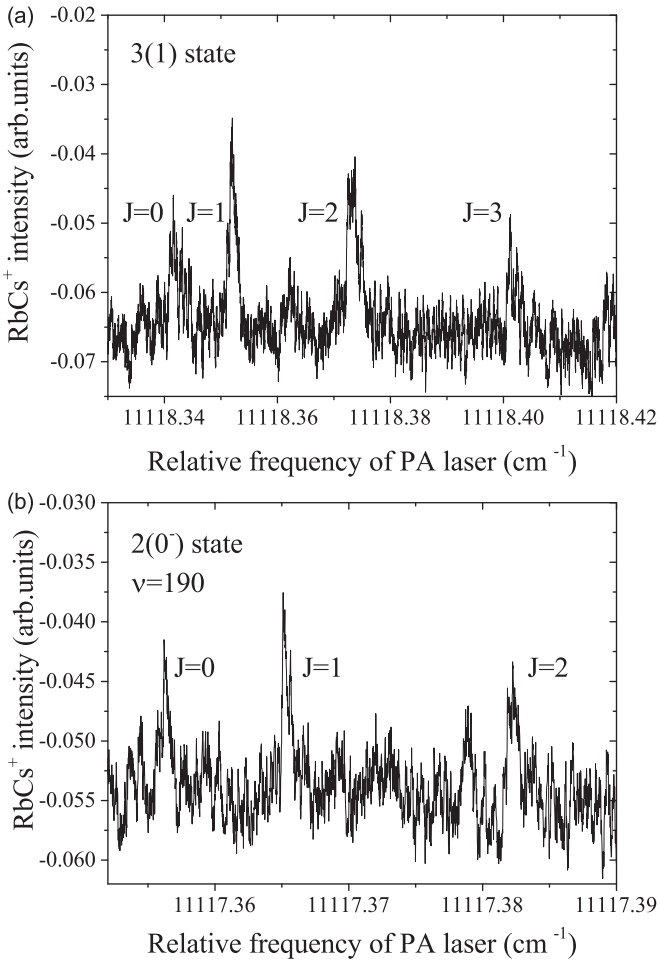

FIG. 6. (a) REMPI spectrum with PA transition to the unassigned perturbing vibrational level of the 3(1) state. (b) REMPI spectrum with PA transition to the $v = 190$ level of the $2(0^-)$ state.

The perturbing vibrational level of the 3(1) state and REMPI spectra of ground-state RbCs molecules formed by PA *via* the $v = 190$ level of the $2(0^-)$ state are illustrated in Figs. 6(a) and 6(b), respectively. Using the method outlined in Refs. [44,45]. The formation rate of ground state RbCs molecules *via* spontaneous emission is estimated on the order of 10^3 molecules/s.

[1] L. D. Carr, D. DeMille, R. V. Krems, and J. Ye, New J. Phys. **11**, 055049 (2009).
[2] O. Dulieu and C. Gabbanini, Rep. Prog. Phys. **72**, 086401 (2009).
[3] M. G. Kozlov and L. N. Labzowsky, J. Phys. B **28**, 1933 (1995).
[4] S. Ospelkaus, K.-K. Ni, D. Wang, M. H. G. de Miranda, B. Neyenhuis, G. Quéméner, P. S. Julienne, J. L. Bohn, D. S. Jin, and J. Ye, Science **327**, 853 (2010).
[5] D. DeMille, Phys. Rev. Lett. **88**, 067901 (2002).
[6] M. Schnell and G. Meijer, Angew. Chem. Int. Ed. **48**, 6010 (2009).

[7] J. Deiglmayr, A. Grochola, M. Repp, K. Mörtlbauer, C. Glück, J. Lange, O. Dulieu, R. Wester, and M. Weidemuller, Phys. Rev. Lett. **101**, 133004 (2008).

[8] S. Dutta, J. Lorenz, A. Altaf, D. S. Elliott, and Y. P. Chen, Phys. Rev. A **89**, 020702(R) (2014).

[9] C. Haimberger, J. Kleinert, M. Bhattacharya, and N. P. Bigelow, Phys. Rev. A **70**, 021402(R) (2004).

[10] D. Wang, J. Qi, M. F. Stone, O. Nikolayeva, H. Wang, B. Hattaway, S. D. Gensemer, P. L. Gould, E. E. Eyler, and W. C. Stwalley, Phys. Rev. Lett. **93**, 243005 (2004).

[11] J. M. Sage, S. Sainis, T. Bergeman, and D. DeMille, Phys. Rev. Lett. **94**, 203001 (2005).

[12] N. Nemitz, F. Baumer, F. Münchow, S. Tassy, and A. Görlitz, Phys. Rev. A **79**, 061403(R) (2009).

[13] A. Ridinger, S. Chaudhuri, T. Salez, D. R. Fernandes, N. Bouloufa, O. Dulieu, C. Salomon, and F. Chevy, Europhys. Lett. **96**, 33001 (2011).

[14] D. DeMille, S. Sainis, J. Sage, T. Bergeman, S. Kotochigova, and E. Tiesinga, Phys. Rev. Lett. **100**, 043202 (2008).

[15] J. Kim, S. Moal, M. Portier, J. Dugué, M. Leduc, and C. Cohen-Tannoudji, Europhys. Lett. **72**, 548 (2005).

[16] P. S. Żuchowski and J. M. Hutson, Phys. Rev. A **81**, 060703(R) (2010).

[17] H. Wang and W. C. Stwalley, J. Chem. Phys. **108**, 5767 (1998).

[18] P. K. Molony, P. D. Gregory, Z. Ji, B. Lu, M. P. Köppinger, C. R. Le Sueur, C. L. Blackley, J. M. Hutson, and S. L. Cornish, Phys. Rev. Lett. **113**, 255301 (2014).

[19] T. Takekoshi, L. Reichsöllner, A. Schindewolf, J. M. Hutson, C. R. Le Sueur, O. Dulieu, F. Ferlaino, R. Grimm, and H. C. Nägerl, Phys. Rev. Lett. **113**, 205301 (2014).

[20] D. J. McCarron, H. W. Cho, D. L. Jenkin, M. P. Köppinger, and S. L. Cornish, Phys. Rev. A **84**, 011603(R) (2011).

[21] A. D. Lercher, T. Takekoshi, M. Debatin, B. Schuster, R. Rameshan, F. Ferlaino, R. Grimm, and H.-C. Nägerl, Eur. Phys. J. D **65**, 3 (2011).

[22] L. D. Marco, G. Valtolina, K. Matsuda, W. G. Tobias, J. P. Covey, and J. Ye, Science **363**, 853 (2019).

[23] A. J. Kerman, J. M. Sage, S. Sainis, T. Bergeman, and D. DeMille, Phys. Rev. Lett. **92**, 153001 (2004).

[24] T. Shimasaki, M. Bellos, C. D. Bruzewicz, Z. Lasner, and D. DeMille, Phys. Rev. A **91**, 021401(R) (2015).

[25] T. Shimasaki, J.-T. Kim, and D. DeMille, Chem. Phys. Chem. **17**, 3677 (2016).

[26] T. Shimasaki, J.-T. Kim, Y. Zhu, and D. DeMille, Phys. Rev. A **98**, 043423 (2018).

[27] D. Comparat, J. Chem. Phys. **120**, 1318 (2004).

[28] A. R. Allouche, M. Korek, K. Fakherddin, A. Chaalan, M. Dagher, F. Taher, and M. Aubert-Frécon, J. Phys. B **33**, 2307 (2000).

[29] H. Fahs, A. R. Allouche, M. Korek, and M. Aubert-Frécon, J. Phys. B **35**, 1501 (2002).

[30] Z. Ji, H. Zhang, J. Wu, J. Yuan, Y. Yang, Y. Zhao, J. Ma, L. Wang, L. Xiao, and S. Jia, Phys. Rev. A **85**, 013401 (2012).

[31] M. H. Anderson, W. Petrich, J. R. Ensher, and E. A. Cornell, Phys. Rev. A **50**, R3597 (1994).

[32] C. G. Townsend, N. H. Edwards, K. P. Zetie, C. J. Cooper, J. Rink, and C. J. Foot, Phys. Rev. A **53**, 1702 (1996).

[33] M. Lysebo and L. Veseth, Phys. Rev. A **77**, 032721 (2008).

[34] Y. Yang and O. Kühn, Mol. Phys. **106**, 2445 (2008).

[35] Y. Yang, D. Jia, Y.-J. Wang, H.-J. Zhai, Y. Man, and S.-D. Li, Nanoscale **9**, 1443 (2017).

[36] A. J. Kerman, J. M. Sage, S. Sainis, T. Bergeman, and D. DeMille, Phys. Rev. Lett. **92**, 033004 (2004).

[37] T. Bergeman, C. E. Fellows, R. F. Gutterres, and C. Amiot, Phys. Rev. A **67**, 050501(R) (2003), and private communication.

[38] R. J. LeRoy and R. B. Bernstein, J. Chem. Phys. **52**, 3869 (1970).

[39] G. Herzberg, *Molecular Spectra and Molecular Structure*. Vol. 1: Spectra of Diatomic Molecules (Academic, New York, 1950).

[40] R. W. Field, S. G. Tilford, R. A. Howard, and J. D. Simmons, J. Mol. Spectrosc. **44**, 347 (1972).

[41] C. Li, L. Deng, Y. Zhang, L. Wu, X. Yang, and Y. Chen, J. Phys. Chem. A **115**, 2978 (2011).

[42] L. B. Hélène and R. W. Field, *The Spectra and Dynamics of Diatomic Molecules* (Academic, Orsay, 2003).

[43] C. Li, L. Deng, J. Zhang, X. Qiu, J. Wei, and Y. Chen, J. Mol. Spectrosc. **284**, 29 (2013).

[44] W. Ketterle, K. B. Davis, M. A. Joffe, A. Martin, and D. E. Pritchard, Phys. Rev. Lett. **70**, 2253 (1993).

[45] Z. Li, T. Gong, Z. Ji, Y. Zhao, L. Xiao, and S. Jia, Phys. Chem. Chem. Phys. **20**, 4893 (2018).